View metadata, citation and similar papers at core.ac.uk

brought to you by CORE

provided by NASA Technical Reports Server

NASA TECHNICAL NOTE

NASA TN D-5900

NASA TN D-5900

c.1

TECH LIBRARY KAFB, NM

0132629

LOAN COPY: RETU
AFWL (WLOL)
KIRTLAND AFB, N

DETERMINATION OF INFLATED SHAPE AND INERTIAL PROPERTIES OF AN ALL-FLEXIBLE PARAWING

by Blair B. Gloss

Langley Research Center
Hampton, Va. 23365

NATIONAL AERONAUTICS AND SPACE ADMINISTRATION • WASHINGTON, D. C. • JULY 1970

TECH LIBRARY KAFB, NM
0132629

1. Report No.	2. Government Accession No.	3. Recipient's Catalog No.
NASA TN D-5900		

4. Title and Subtitle

DETERMINATION OF INFLATED SHAPE AND INERTIAL PROPERTIES OF AN ALL-FLEXIBLE PARAWING

5. Report Date: July 1970

6. Performing Organization Code:

7. Author(s)

Blair B. Gloss

8. Performing Organization Report No.: L-6906

9. Performing Organization Name and Address

NASA Langley Research Center
Hampton, Va. 23365

10. Work Unit No.: 126-13-10-03

11. Contract or Grant No.:

12. Sponsoring Agency Name and Address

National Aeronautics and Space Administration
Washington, D.C. 20546

13. Type of Report and Period Covered: Technical Note

14. Sponsoring Agency Code:

15. Supplementary Notes

16. Abstract

The inflated shape of a single-keel, all-flexible parawing with a 45° leading-edge sweep and a 5-foot (1.52-meter) keel length has been determined by using a photogrammetric technique. The shape of this parawing was determined at lift-drag ratios of 2.13, 2.24, and 2.43 with the wing in tethered flight in a wind tunnel. The shape data for the inflated parawing showed a 3.0-percent increase in the span and a 3.0-percent decrease in the keel length when the lift-drag ratio increased from 2.13 to 2.43. The nondimensional inertial properties and center-of-gravity locations of the parawing structure were calculated from the shape data. The inertial properties and center-of-gravity locations calculated for a geometrically similar parawing with a 24-foot (7.32-meter) keel length were in excellent agreement with measured values obtained from pendulum tests.

17. Key Words (Suggested by Author(s))

Parawing
Flexible wing
Inertia
Shape

18. Distribution Statement

Unclassified – Unlimited

19. Security Classif. (of this report)	20. Security Classif. (of this page)	21. No. of Pages	22. Price*
Unclassified	Unclassified	31	$3.00

*For sale by the Clearinghouse for Federal Scientific and Technical Information
Springfield, Virginia 22151

DETERMINATION OF INFLATED SHAPE AND INERTIAL PROPERTIES OF AN ALL-FLEXIBLE PARAWING

By Blair B. Gloss
Langley Research Center

SUMMARY

The inflated shape of a single-keel, all-flexible parawing with a 45° leading-edge sweep and a 5-foot (1.52-meter) keel length has been determined by using a photogrammetric technique. The shape of this parawing was determined at lift-drag ratios of 2.13, 2.24, and 2.43 with the wing in tethered flight in a wind tunnel. For the inflated parawing, the span increased 3.0 percent and the keel length decreased 3.0 percent when the lift-drag ratio increased from 2.13 to 2.43.

Nondimensional inertial properties were calculated from the shape data. These nondimensional inertias can be scaled to any geometrically similar single-keel, all-flexible parawing with a 45° leading-edge sweep and with any weight canopy and any weight suspension lines. The center of gravity of the system was calculated from the shape data and was found to rotate about the confluence point with changes in lift-drag ratio.

INTRODUCTION

The National Aeronautics and Space Administration is continuing the investigation of parawings in order to develop parawing technology more fully and to gain an understanding of their aerodynamic characteristics. (See ref. 1.) Because the shape of all-flexible parawings in gliding flight has not been numerically defined, an aerodynamic analysis of the parawing could not be made. The only way of determining inertial properties (both structural and apparent mass) was to swing the parawing, suspended on a frame to approximate the inflated parawing shape, in a vacuum sphere. (See ref. 2.) The structural inertias were determined by swinging the parawing in a vacuum, and the apparent-mass inertias were determined by considering the results of swinging the parawing in a vacuum and at atmospheric conditions. The present investigation was undertaken to determine the shape and structural inertial properties of an all-flexible parawing by using a photogrammetric technique. In contrast with the swinging technique, which uses only the approximate shape of the parawing and does not provide the products of inertia, the photogrammetric technique enables determination of the inflated shape of the parawing, from which the moments and products of inertia can be obtained.

The inflated shape of a single-keel, all-flexible parawing with a 45° leading-edge sweep and a 5-foot (1.52-meter) keel length was determined at lift-drag ratios of 2.13, 2.24, and 2.43 while the parawing was flying tethered in the 17-foot (5.18-meter) test section of the Langley 300-MPH 7- by 10-foot tunnel. The measured shape data were used to obtain nondimensional structural inertial properties of the parawing. Because there was no convenient reference chord for measuring the angle of attack of a parawing in tethered flight, lift-drag ratio rather than the angle of attack was used to define the model test condition.

SYMBOLS

A,B,C	constants in equation of a plane
a	cross-sectional area of suspension line, ft^2 (m^2)
b	distance between lenses of stereo cameras, ft (m)
c	focal length of lenses of stereo cameras, ft (m)
d	distance from projection of point in $X_S Z_S$-plane to $X_t Z_t$-plane, ft (m)
I_{XX}	rolling moment of inertia in confluence-point axis system, slug-ft^2 (kg-m^2)
I_{YY}	pitching moment of inertia in confluence-point axis system, slug-ft^2 (kg-m^2)
I_{ZZ}	yawing moment of inertia in confluence-point axis system, slug-ft^2 (kg-m^2)
I_{XY}, I_{XZ}, I_{YZ}	products of inertia in confluence-point axis system, slug-ft^2 (kg-m^2)
L/D	lift-drag ratio
l	length of suspension line, ft (m)
l_k	keel length of flat canopy, ft (m)
$l_{k,i}$	keel length of inflated canopy, ft (m)
$l_{s,i}$	span of inflated canopy, ft (m)

m mass of small element of canopy material, slugs (kg)

m_t total mass, slugs (kg)

m' mass per unit area of canopy material, slugs/ft^2 (kg/m^2)

N total number of points read

R $x_{g,L} - x_{g,R}$, ft (m)

X_{cg},Y_{cg},Z_{cg} coordinates of composite center-of-gravity location, ft (m)

x,y,z coordinates of a point with respect to confluence-point axis system, ft (m)

$x_{cg,l},y_{cg,l},z_{cg,l}$ coordinates of center of gravity of a suspension line, ft (m)

x_g,z_g coordinates of a point with respect to glass-plate axis system, ft (m)

x_h,z_h coordinates of a point with respect to comparator-table axis system, ft (m)

$x_{h,g},z_{h,g}$ coordinates of origin of glass-plate axis system with respect to comparator-table axis system, ft (m)

x_k distance from wing apex along keel, ft (m)

x_{le} distance from wing apex along leading edge, ft (m)

x_s,y_s,z_s coordinates of a point with respect to stereo-camera axis system, ft (m)

x_t,y_t,z_t coordinates of a point with respect to tunnel axis system, ft (m)

$x_{t,cp},y_{t,cp},z_{t,cp}$ coordinates of origin of confluence-point axis system with respect to tunnel axis system, ft (m)

α,ϕ,θ direction angles of suspension line (fig. 7), deg

γ rotation angle of glass plate on comparator table, deg

ρ density of suspension line, slugs/ft^3 (kg/m^3)

Subscripts:

c	canopy
cg	center of gravity
i	summation index
L	left plate
le	leading edge
ℓ	line
R	right plate
1,2,3	ceiling reference point when associated with coordinates; coordinate plane when associated with A, B, and C

Bar over a symbol represents a nondimensional value.

MODEL

The flat planform of the canopy and suspension-line lengths of the parawing that was used in this investigation are shown in figure 1 and table I, respectively. The lines were 130-pound (578-newton) test dacron. The wing was constructed of white rip-stop nylon fabric which had a unit weight of 1.1 oz/yd^2 (37 g/m^2). The fabric had been made nonporous by an acrylic coating to obtain maximum aerodynamic efficiency of the parawing. All seams were glued rather than sewed to insure the desired dimensional accuracy by avoiding gathering of the material which always occurs in a sewn seam.

A grid pattern of 1-inch-square (2.54-cm) blocks with identification marks every 0.5 inch (1.27 cm) was printed on the underside of the canopy as shown in figure 2. This grid pattern made it possible to locate and identify the same points on each of the pictures taken by the stereo cameras.

TEST FACILITY AND EQUIPMENT

Wind-tunnel tests were conducted in the 17-foot (5.18-meter) test section of the Langley 300-MPH 7- by 10-foot tunnel. Black reference crossmarks, 0.5 inch (1.27 cm)

wide, were painted on the test section ceiling every foot (0.31 meter) on centers as shown in figure 3.

The wing was attached to a strain-gage balance by means of a T-bar (fig. 4). All the suspension lines were held by the line clamp except for the two wing-tip and aft-keel lines, which were tied to the crossbar as shown in figures 3, 4, and 5 in order to stabilize the model in pitch and roll.

The stereo camera system is shown installed in the test section in figures 3 and 5. This system consisted of two camera units mounted rigidly 1.31 feet (0.39 meter) apart with parallel optical axes. Each camera had a focal length of 0.20 foot (0.06 meter). Because these cameras had very high quality lenses, no correction was made for lens distortion. The cameras were electrically operated so that the shutters on both cameras were opened simultaneously. The pictures were taken on sensitized glass plates, which are structurally more stable than film. Four fiducial marks were put on each sensitized glass plate while it was still in the camera by exposing it to radium.

TEST CONDITIONS AND CORRECTIONS

Static wind-tunnel tests were conducted at a dynamic pressure of 0.5 lb/ft^2 (23.9 N/m^2). Jet-boundary corrections to drag coefficient, as determined from reference 3, have been applied to the wind-tunnel results. The ratio of the wing area to the cross-sectional area of the test section was small; therefore, no blockage corrections were made to the dynamic pressure.

The lift-drag ratio was varied by shortening the eleventh keel line (table I) while the support sting remained at an angle of attack of 0^o. Because there was no convenient reference chord for measuring the angle of attack of a parawing in tethered flight, lift-drag ratio rather than the angle of attack was used to define the model test condition. Line lengths were measured immediately after each test.

SHAPE MEASUREMENTS

A stereo-optic film reader was used to read each set of photographs (glass plates). These plates were read by locating the same point on each photograph and determining the coordinates of that point with respect to a set of axes on each plate. Because the parawing was always assumed to be symmetric about its keel, only half of the parawing was read. The corners of the grid intersections on the parawing (fig. 2), the suspension-line-attachment points on the canopy, and the confluence point of the lines were read. Thus, all points that were read were either centers of adjoining elements of material 1 in^2 (6.45 cm^2) in area, line-attachment points on the canopy, or the confluence point. At the

boundaries, however, the points that were read were not centers of squares, but they were assumed to be centers of odd-shaped pieces of material, the sizes of which were estimated as each point was read. (See fig. 2.)

The equations used to calculate the coordinates of the inflated parawing are presented in the appendix. The appendix includes equations for transforming comparator-table coordinates to glass-plate coordinates; two-dimensional, glass-plate coordinates to three-dimensional camera coordinates; camera coordinates to tunnel coordinates; and tunnel coordinates to confluence-point coordinates. A sketch showing the axes systems used in the transformation from camera to confluence-point coordinates is presented in figure 6.

ACCURACY OF SHAPE DATA

The accuracy of the shape data was checked by comparing the measured distances between the centers of the painted crossmarks on the ceiling, shown in figure 3, with the calculated distances. The calculated distances were within about 3 percent of the measured values, the chief source of error being the inability to read accurately the center of the crossmarks. Because the grid on the wing was much narrower than the ceiling crossmarks, the centers of the grid intersections were easier to determine and the accuracy of the parawing-shape data should be better than the 3-percent accuracy of the ceiling crossmarks.

INERTIAL PROPERTIES

Once an accurate description of the shape of the inflated parawing has been determined, the moments of inertia of the canopy can be computed by mathematically dividing the wing into small elements, determining the mass and radius of gyration of each element, and summing the computed moments of inertia of each element about the origin of the confluence-point coordinate system shown in figure 6.

By using the following equations, the nondimensional moments and products of inertia (see ref. 4) were calculated for the canopy:

$$\bar{I}_{XX,c} = \frac{I_{XX,c}}{m' l_k^4} = \frac{2}{m' l_k^2} \sum_{i=1}^{N} \left[\left(\frac{y}{l_k} \right)^2 m + \left(\frac{z}{l_k} \right)^2 m \right]_i \tag{1}$$

$$\bar{I}_{YY,c} = \frac{I_{YY,c}}{m' l_k^4} = \frac{2}{m' l_k^2} \sum_{i=1}^{N} \left[\left(\frac{x}{l_k} \right)^2 m + \left(\frac{z}{l_k} \right)^2 m \right]_i \tag{2}$$

$$\bar{I}_{ZZ,c} = \frac{I_{ZZ,c}}{m' l_k^4} = \frac{2}{m' l_k^2} \sum_{i=1}^{N} \left[\left(\frac{x}{l_k} \right)^2 m + \left(\frac{y}{l_k} \right)^2 m \right]_i \tag{3}$$

$$\bar{I}_{XZ,c} = \frac{I_{XZ,c}}{m' l_k^4} = \frac{2}{m' l_k^2} \sum_{i=1}^{N} \left(\frac{x}{l_k} \frac{y}{l_k} m \right)_i \tag{4}$$

$$\bar{I}_{XY,c} = 0 \tag{5}$$

$$\bar{I}_{YZ,c} = 0 \tag{6}$$

In equations (1) to (6), N is the total number of points read and x, y, and z are the coordinates of the center of each small piece of canopy material. The terms that are summed are either the moments or products of inertia of each small piece of material.

The coordinates of each end of all the lines were determined; therefore, the length of each line was calculated. By using the following equations, the moments and products of inertia for all the lines were calculated:

$$\bar{I}_{XX,l} = \frac{I_{XX,l}}{\rho a l_k^3} = \frac{1}{3} \sum_{i=1}^{23} \left[\left(\sin^2\phi + \sin^2\theta \right) \left(\frac{l}{l_k} \right)^3 \right]_i \tag{7}$$

$$\bar{I}_{YY,l} = \frac{I_{YY,l}}{\rho a l_k^3} = \frac{1}{3} \sum_{i=1}^{23} \left[\left(\sin^2\alpha + \sin^2\theta \right) \left(\frac{l}{l_k} \right)^3 \right]_i \tag{8}$$

$$\bar{I}_{ZZ,l} = \frac{I_{ZZ,l}}{\rho a l_k^3} = \frac{1}{3} \sum_{i=1}^{23} \left[\left(\sin^2\alpha + \sin^2\phi \right) \left(\frac{l}{l_k} \right)^3 \right]_i \tag{9}$$

$$\bar{I}_{XZ,l} = \frac{I_{XZ,l}}{\rho a l_k^3} = \frac{1}{3} \sum_{i=1}^{23} \left[(\sin \phi \sin \theta) \left(\frac{l}{l_k} \right)^3 \right]_i \tag{10}$$

$$\bar{I}_{XY,l} = 0 \tag{11}$$

$$\bar{I}_{YZ,l} = 0 \tag{12}$$

Angles α, θ, and ϕ are defined in figure 7. The terms in the brackets are either the moments or the products of inertia of an individual line.

Table II presents the nondimensional structural inertias calculated for lift-drag ratios of 2.13, 2.24, and 2.43.

The following equations can be used to calculate the pitching moments of inertia for the canopy and suspension lines, respectively, for a geometrically similar parawing flying at a lift-drag ratio of 2.13.

$$I_{YY,c} = 1.144 m' l_k^4 \tag{13}$$

$$I_{YY,l} = 14.54 \rho a l_k^3 \tag{14}$$

where the constants are from table II.

DETERMINATION OF CENTER-OF-GRAVITY LOCATIONS

The center-of-gravity location (see ref. 4) of the canopy was calculated by using the following equations:

$$\bar{X}_{cg,c} = \frac{X_{cg,c}}{l_k} = \frac{2 \sum_{i=1}^{N} \left(\frac{x}{l_k} m \right)_i}{m_{t,c}} \tag{15}$$

$$\bar{Y}_{cg,c} = \frac{Y_{cg,c}}{l_k} = \frac{2 \sum_{i=1}^{N} \left(\frac{y}{l_k} m \right)_i}{m_{t,c}} \tag{16}$$

$$\overline{Z}_{cg,c} = \frac{Z_{cg,c}}{l_k} = \frac{2\sum_{i=1}^{N}\left(\frac{z}{l_k}\,m\right)_i}{m_{t,c}} \tag{17}$$

where x, y, and z are the coordinates of the center of each small piece of material.

The composite center-of-gravity location of the lines was calculated by using the following equations:

$$\overline{X}_{cg,l} = \frac{X_{cg,l}}{l_k} = \frac{\sum_{i=1}^{23}\left(\frac{x_{cg,l}}{l_k}\,\rho a l\right)_i}{m_{t,l}} \tag{18}$$

$$\overline{Y}_{cg,l} = \frac{Y_{cg,l}}{l_k} = \frac{\sum_{i=1}^{23}\left(\frac{y_{cg,l}}{l_k}\,\rho a l\right)_i}{m_{t,l}} \tag{19}$$

$$\overline{Z}_{cg,l} = \frac{Z_{cg,l}}{l_k} = \frac{\sum_{i=1}^{23}\left(\frac{z_{cg,l}}{l_k}\,\rho a l\right)_i}{m_{t,l}} \tag{20}$$

In these equations $x_{cg,l}$, $y_{cg,l}$, and $z_{cg,l}$ are the coordinates of the center of gravity of each suspension line.

Table II presents the calculated nondimensional center-of-gravity coordinates for lift-drag ratios of 2.13, 2.24, and 2.43.

RESULTS AND DISCUSSION

Parawing Shape

Each set of glass plates was read for lift-drag ratios of 2.13, 2.24, and 2.43. As shown in figure 8, the inflated keel length decreased 3 percent and the inflated span increased 3 percent when the lift-drag ratio increased from 2.13 to 2.43. The aspect ratio, which was based on the projected area of the wing and the inflated span, remained constant at 1.96.

The streamwise sections of the wing were obtained by choosing a distance from the keel y and finding the corresponding x and z coordinates from the calculated data.

If enough coordinates to define the shape of a section were not found, linear interpolations between points which had y values close to the selected value were used to find the coordinates that were needed. Few interpolations were necessary. Figure 9 shows typical streamwise sections of a parawing flying at a lift-drag ratio of 2.24.

When the plates were read, no attempt was made to read small wrinkles in the canopy; therefore, the streamwise sections shown in figure 9 are fairly smooth. Section 6, however, has a deep wrinkle due to the nearby attachment of a canopy suspension line. Section 8 is closed because the wing tips (last lines on the leading edges) doubled back under the canopy. Careful examination of figure 3 indicates that closed sections were possible and were, in fact, to be expected. As can be concluded from figure 9, this parawing has extremely large amounts of dihedral, twist, and camber.

Parawing Inertial Properties

When the lift-drag ratio increased from 2.13 to 2.43, the following changes in the structural inertial properties of the canopy were noted: $\bar{I}_{XX,c}$ increased about 5 percent, $\bar{I}_{YY,c}$ remained nearly constant, $\bar{I}_{ZZ,c}$ decreased about 18 percent, and $\bar{I}_{XZ,c}$ decreased about 9 percent. When the lift-drag ratio increased from 2.13 to 2.43, the following changes in the structural inertial properties of the lines were noted: $\bar{I}_{XX,l}$ increased about 6 percent, $\bar{I}_{YY,l}$ increased about 2 percent, $\bar{I}_{ZZ,l}$ decreased about 19 percent, and $\bar{I}_{XZ,l}$ decreased about 10 percent. Figure 10 shows that the wing essentially rotated about its confluence point with changes in lift-drag ratio. This rotation is primarily responsible for the changes in $\bar{I}_{XX}$, $\bar{I}_{ZZ}$, and $\bar{I}_{XZ}$.

Comparison of Two Techniques of Determining Inertial Properties

The pitching and rolling moments of inertia and the center of gravity for a single-keel, all-flexible parawing with a 45° leading-edge sweep and a 24-foot (7.32-meter) keel length were determined by using the pendulum method as outlined in reference 2. The mass per unit length of the suspension lines of this parawing was 0.00032 slug/ft (15 g/m), and the average mass per unit area of the canopy material, including line-attachment points, was 6.18 oz/yd^2 (210 g/m^2). In order to facilitate comparison of the pendulum technique of determining inertial properties with the photogrammetric technique, the data from the present investigation of a geometrically similar parawing with a 5-foot (1.52-meter) keel length were scaled to the 24-foot (7.32-meter) parawing. There were a few differences between the scaled-up parawing and the actual 24-foot parawing. The suspension lines on the scaled-up parawing were generally 1 foot (0.31 meter) longer than those of the 24-foot parawing, but the 24-foot parawing had a 1.1-foot (0.34-meter), 1.5-pound (680-gram) riser attached to the lines, which moved the canopy to about the right distance from the rotation point to allow comparison.

The following table presents the results from the two techniques of determining the inertial properties:

Moment of inertia	Photogrammetric method		Pendulum method	
	slug-ft^2	kg-m^2	slug-ft^2	kg-m^2
I_{XX}	578	784	502	681
I_{YY}	569	771	501	679

Figure 11 shows both the photogrammetrically determined and the estimated (ref. 2) center-of-gravity locations of the 24-foot (7.32-meter) parawing.

CONCLUDING REMARKS

The inflated shape of a single-keel, all-flexible parawing with a 45° leading-edge sweep and a 5-foot (1.52-meter) keel length were determined by using a photogrammetric technique. Nondimensional inertial properties and center-of-gravity locations were calculated from the shape data. The present investigation has shown that neither the inertial properties nor the center-of-gravity locations can be assumed to be constant with changes in lift-drag ratio. The inertial properties and center-of-gravity locations of a geometrically similar parawing with a 24-foot (7.32-meter) keel length were calculated from the photogrammetric data. The results were in excellent agreement with measured values obtained from pendulum tests.

Langley Research Center,
National Aeronautics and Space Administration,
Hampton, Va., May 12, 1970.

APPENDIX

TRANSFORMATION EQUATIONS

The inflated canopy shape of the parawing used in this investigation was determined by photographing the parawing with a stereo camera system which used sensitized glass plates rather than film. The comparator-table coordinates x_h,z_h of wing-grid points on the glass plates were read on a stereo-optic film reader and transformed to the confluence-point coordinates x,y,z of the wing in the tunnel. (See fig. 6.) This appendix explains the methods and lists the equations used in the transformation of coordinates.

Transformation From Comparator-Table to Glass-Plate Coordinates

No special care was taken in alining each photograph (glass plate) on the comparator table since the plates were read individually and not in the usual stereo fashion, in which the subject is optically alined in stereo and the coordinates of the same point on each plate are read. The coordinate systems of the right and left glass plates were alined by mathematically translating and rotating the axes so that the coordinates of the comparator table x_h,z_h and the coordinates of each glass plate x_g,z_g coincided. Figure 12 shows a typical comparator-table setup. The following transformation equations were used to translate and rotate the coordinates of the glass plates:

$$x_g = \left(x_h - x_{h,g}\right)\cos\gamma + \left(z_h - z_{h,g}\right)\sin\gamma \tag{A1}$$

$$z_g = \left(z_h - z_{h,g}\right)\cos\gamma - \left(x_h - x_{h,g}\right)\sin\gamma \tag{A2}$$

Transformation From Glass-Plate to Camera Coordinates

Figure 13 shows the geometric relationship between the two-dimensional coordinates of the right and left glass plates and the three-dimensional camera coordinates x_s,y_s,z_s. For a given point on the wing surface, the following ratios are equal:

$$\frac{y_s}{c} = \frac{z_s}{z_{g,L}} = \frac{x_s}{x_{g,L}} = \frac{b}{R} \tag{A3}$$

where $R = x_{g,L} - x_{g,R}$, b is the distance between the centers of the left and right lenses, and c is the focal length of the lenses. The ratios of equation (A3) can be rearranged to transform glass-plate coordinates to camera coordinates.

$$x_s = \frac{b}{R} x_{g,L} \tag{A4}$$

$$y_s = \frac{bc}{R} \tag{A5}$$

$$z_s = \frac{b}{R} z_{g,L} \tag{A6}$$

Transformation From Camera to Tunnel Coordinates

Because the three-dimensional camera coordinates x_s,y_s,z_s were not particularly convenient to work with, a method for transforming to tunnel coordinates x_t,y_t,z_t was developed. Three of the painted crossmarks on the tunnel ceiling (fig. 6) were chosen as reference points in the tunnel-axis system. Points 1 and 2 were chosen so that a line connecting them, the X_t-axis, was parallel to the wind direction and in the ceiling plane. Point 3 was chosen so that a line connecting points 1 and 3, the Y_t-axis, was perpendicular to the X_t-axis and in the ceiling plane. The Z_t-axis was perpendicular to the ceiling plane at point 1. The tunnel coordinates of a point given in camera coordinates were determined by solving three sets of three simultaneous equations for the constants of the equations defining the planes formed by the tunnel-axis system and then calculating the distance from the point to each of the tunnel-axes planes. (See refs. 5 and 6.)

In the X_tY_t-plane, the constants A, B, and C were determined from the following set of equations:

$$\left.\begin{aligned} Ax_{s,1} + By_{s,1} + Cz_{s,1} + 1 = 0 \\ Ax_{s,2} + By_{s,2} + Cz_{s,2} + 1 = 0 \\ Ax_{s,3} + By_{s,3} + Cz_{s,3} + 1 = 0 \end{aligned}\right\} \tag{A7}$$

In the Y_tZ_t-plane, the following set of equations was solved for A_1, B_1, and C_1:

$$\left.\begin{aligned} A_1A + B_1B + C_1C = 0 \\ A_1x_{s,1} + B_1y_{s,1} + C_1z_{s,1} + 1 = 0 \\ A_1x_{s,3} + B_1y_{s,3} + C_1z_{s,3} + 1 = 0 \end{aligned}\right\} \tag{A8}$$

The constants A_2, B_2, and C_2 in the X_tZ_t-plane were determined from the third set of equations:

$$\left.\begin{aligned} A_2A + B_2B + C_2C &= 0 \\ A_2x_{s,1} + B_2y_{s,1} + C_2z_{s,1} + 1 &= 0 \\ A_2x_{s,2} + B_2y_{s,2} + C_2z_{s,2} + 1 &= 0 \end{aligned}\right\} \tag{A9}$$

The distance from a point x_s,y_s,z_s to the Y_tZ_t-plane is

$$x_t = \frac{\left|A_1x_s + B_1y_s + C_1z_s\right|}{\sqrt{A_1^2 + B_1^2 + C_1^2}} \tag{A10}$$

The distance to the X_tZ_t-plane is

$$y_t = \frac{\left|A_2x_s + B_2y_s + C_2z_s\right|}{\sqrt{A_2^2 + B_2^2 + C_2^2}} \tag{A11}$$

The distance to the X_tY_t-plane is

$$z_t = \frac{\left|Ax_s + By_s + Cz_s\right|}{\sqrt{A^2 + B^2 + C^2}} \tag{A12}$$

Equations (A10), (A11), and (A12) were used to transform the camera coordinates of a point to tunnel coordinates. To determine the sign of the y_t coordinate of a point, the distance from the projection of the point in the X_sZ_s-plane to the X_tZ_t-plane was calculated by using the following equation:

$$d = \frac{-\left(C_2z_s + A_2x_s + 1\right)}{B_2} \tag{A13}$$

If y_s was greater than d, the point was located beyond the X_tZ_t-plane in relation to the X_sZ_s-plane and y_t was therefore chosen as positive. If y_s was less than d, y_t was negative.

Transformation From Tunnel to Confluence-Point Coordinates

The shape and inertial data presented in this report were calculated with respect to the confluence-point axis system X,Y,Z as shown in figure 6. The origin of this system was chosen at the confluence point of the suspension lines held by the line clamp. The X- and Y-axis were parallel to and in the same direction as the X_t- and Y_t-axis, respectively. The Z-axis was parallel to but in the opposite direction as the Z_t-axis. The following equations were used to transform a point given in tunnel coordinates to confluence-point coordinates:

$$x = x_t - x_{t,cp} \tag{A14}$$

$$y = y_t - y_{t,cp} \tag{A15}$$

$$z = z_{t,cp} - z_t \tag{A16}$$

where $x_{t,cp}, y_{t,cp}, z_{t,cp}$ are the coordinates of the confluence point.

REFERENCES

1. Naeseth, Rodger L.; and Fournier, Paul G.: Low-Speed Wind-Tunnel Investigation of Tension-Structure Parawings. NASA TN D-3940, 1967.

2. Sumners, Dan O.: Inertia Tests of a 24 Foot Single-Keel Parawing – Model 1. NASA CR-66744, 1968.

3. Gillis, Clarence L.; Polhamus, Edward C.; and Gray, Joseph L., Jr.: Charts for Determining Jet-Boundary Corrections for Complete Models in 7- by 10-Foot Closed Rectangular Wind Tunnels. NACA WR L-123, 1945. (Formerly NACA ARR L5G31.)

4. Pletta, Dan H.; and Frederick, Daniel: Engineering Mechanics – Statics and Dynamics. Ronald Press Co., c.1964.

5. McCoy, Neal H.; and Johnson, Richard E.: Analytic Geometry. Holt, Rinehart and Winston, Inc., c.1955.

6. Wilson, W. A.; and Tracey, J. I.: Analytic Geometry. Third ed., D. C. Heath and Co., c.1949.

TABLE I.- NONDIMENSIONAL LINE LENGTH

Line	L/D	l/l_k		
		Keel	Right leading edge	Left leading edge
1		1.350	1.367	1.365
2		1.360	1.304	1.300
3		1.352	1.258	1.260
4		1.340	1.202	1.215
5		1.323	1.166	1.144
6		1.306	.994	.983
7		1.292		
8		1.269		
9		1.242		
10		1.205		
11	2.42	1.092		
11	2.24	1.075		
11	2.13	1.067		

TABLE II.- NONDIMENSIONAL INERTIAL AND CENTER-OF-GRAVITY DATA

(a) Inertial properties of canopy

L/D	$\bar{I}_{XX,c}$	$\bar{I}_{YY,c}$	$\bar{I}_{ZZ,c}$	$\bar{I}_{XZ,c}$	$\bar{I}_{ZY,c}$	$\bar{I}_{XY,c}$
2.13	0.9304	1.144	0.2957	0.4512	0	0
2.24	.9347	1.149	.2889	.4505	0	0
2.43	.9734	1.143	.2431	.4124	0	0

(b) Inertial properties of lines

L/D	$\bar{I}_{XX,l}$	$\bar{I}_{YY,l}$	$\bar{I}_{ZZ,l}$	$\bar{I}_{XZ,l}$	$\bar{I}_{ZY,l}$	$\bar{I}_{XY,l}$
2.13	12.52	14.54	2.799	4.952	0	0
2.24	12.61	14.55	2.728	4.881	0	0
2.43	13.28	14.81	2.282	4.465	0	0

(c) Center-of-gravity coordinates of lines and canopy

L/D	$\bar{X}_{cg,l}$	$\bar{Y}_{cg,l}$	$\bar{Z}_{cg,l}$	$\bar{X}_{cg,c}$	$\bar{Y}_{cg,c}$	$\bar{Z}_{cg,c}$
2.13	0.241	0	0.550	0.592	0	1.131
2.24	.237	0	.560	.586	0	1.133
2.43	.210	0	.575	.529	0	1.164

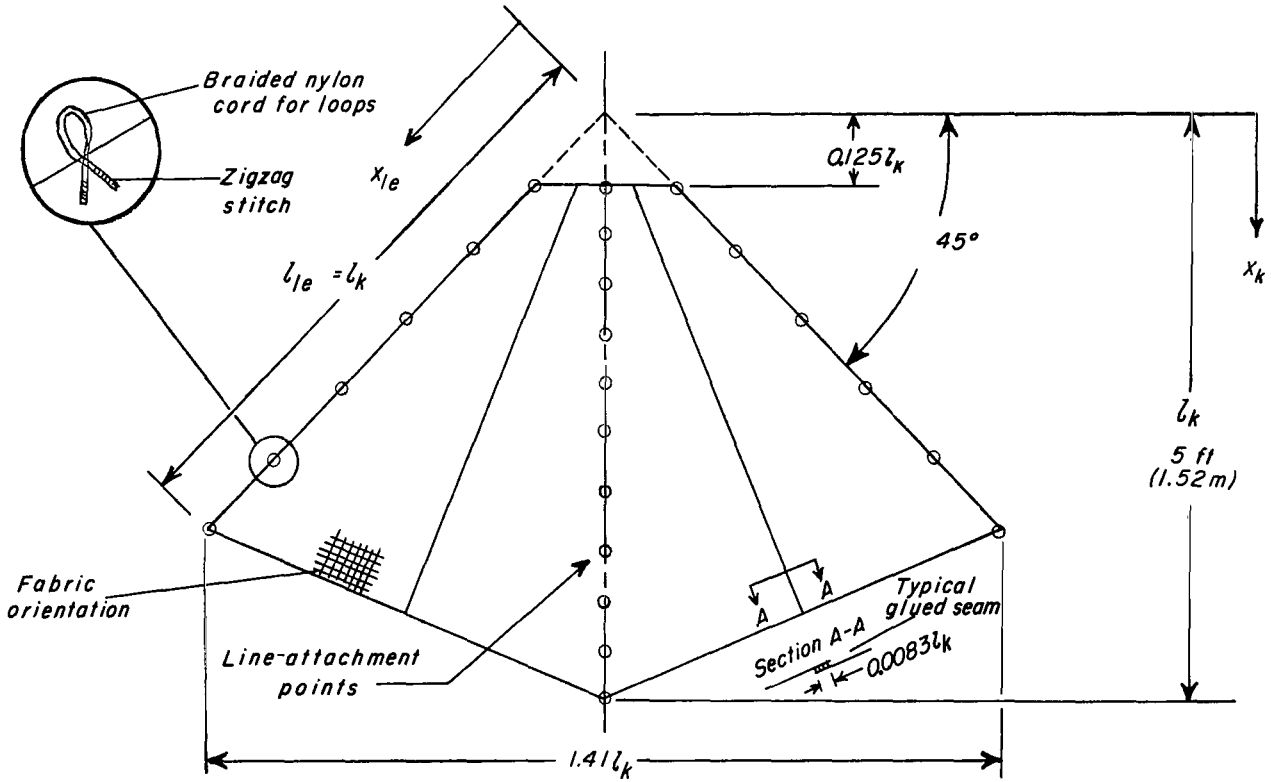

Line-attachment locations

Line	x_k/l_k	x_{le}/l_k
1	0.125	0.177
2	.208	.333
3	.292	.500
4	.375	.667
5	.459	.833
6	.542	1.000
7	.645	
8	.750	
9	.833	
10	.917	
11	1.000	

Figure 1.- Planform details of the parawing.

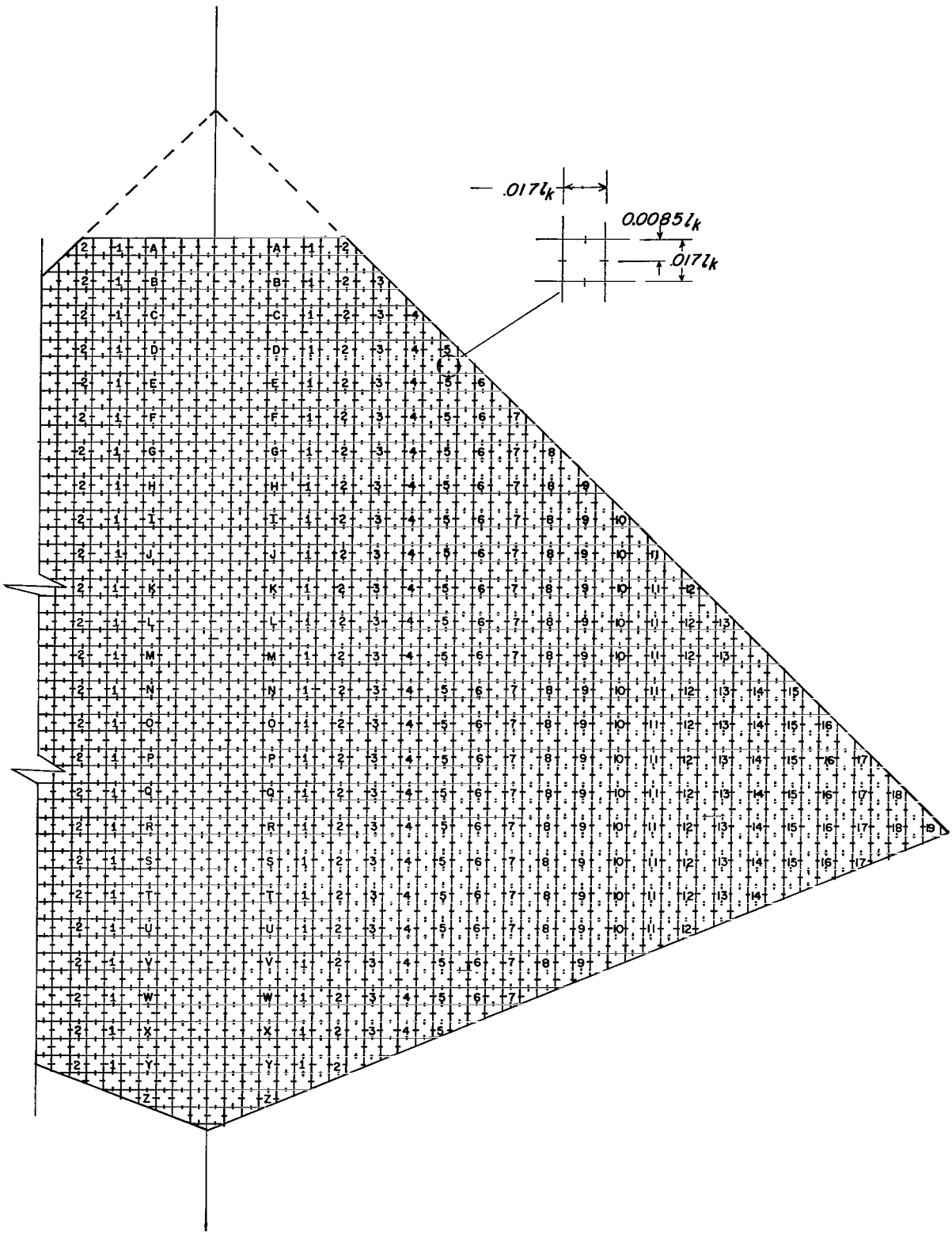

Figure 2.- Canopy grid system.

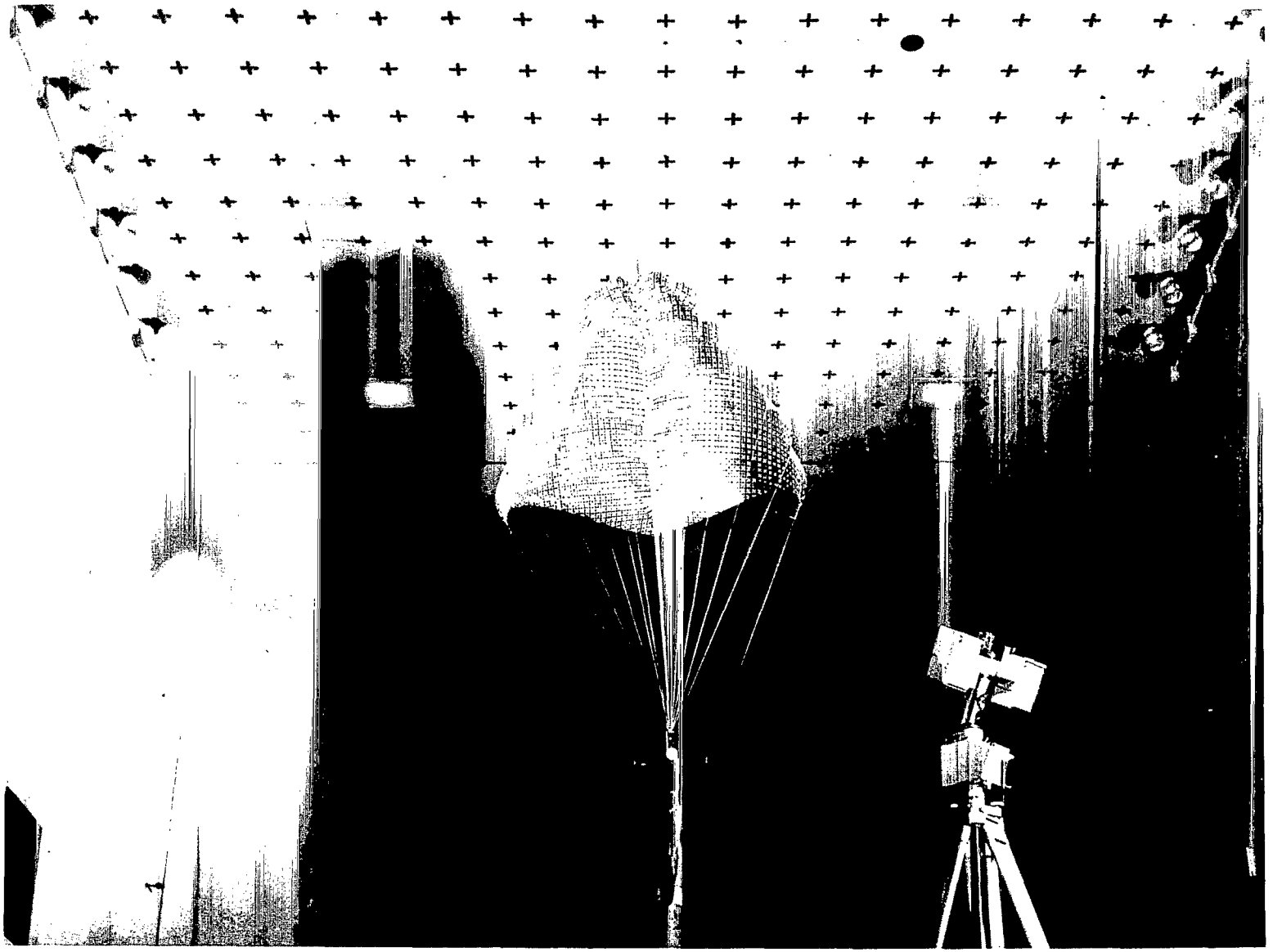

Figure 3.- Front view of setup for wind-tunnel tests. L-68-10 794

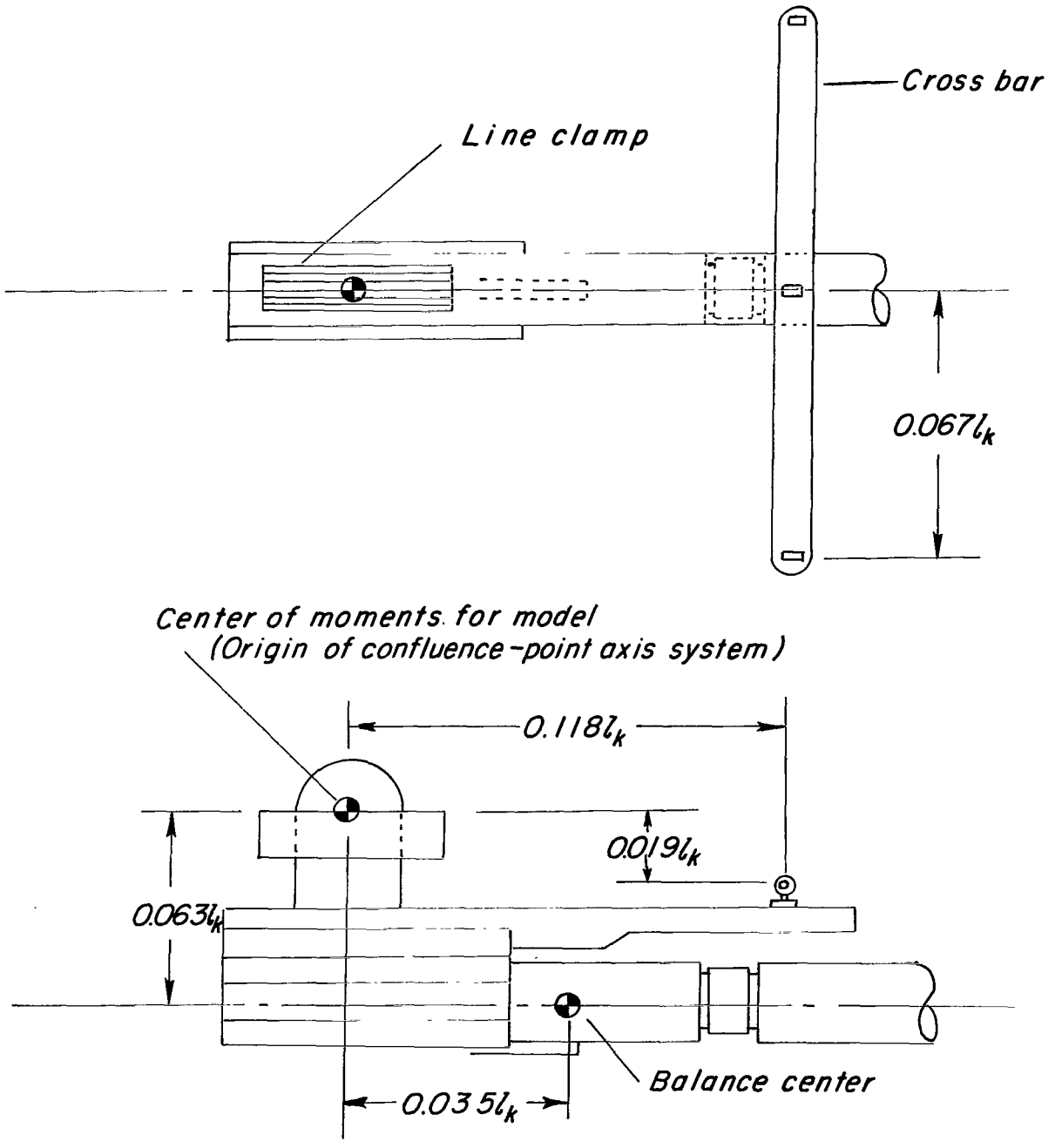

Figure 4.- T-bar used in wind-tunnel tests.

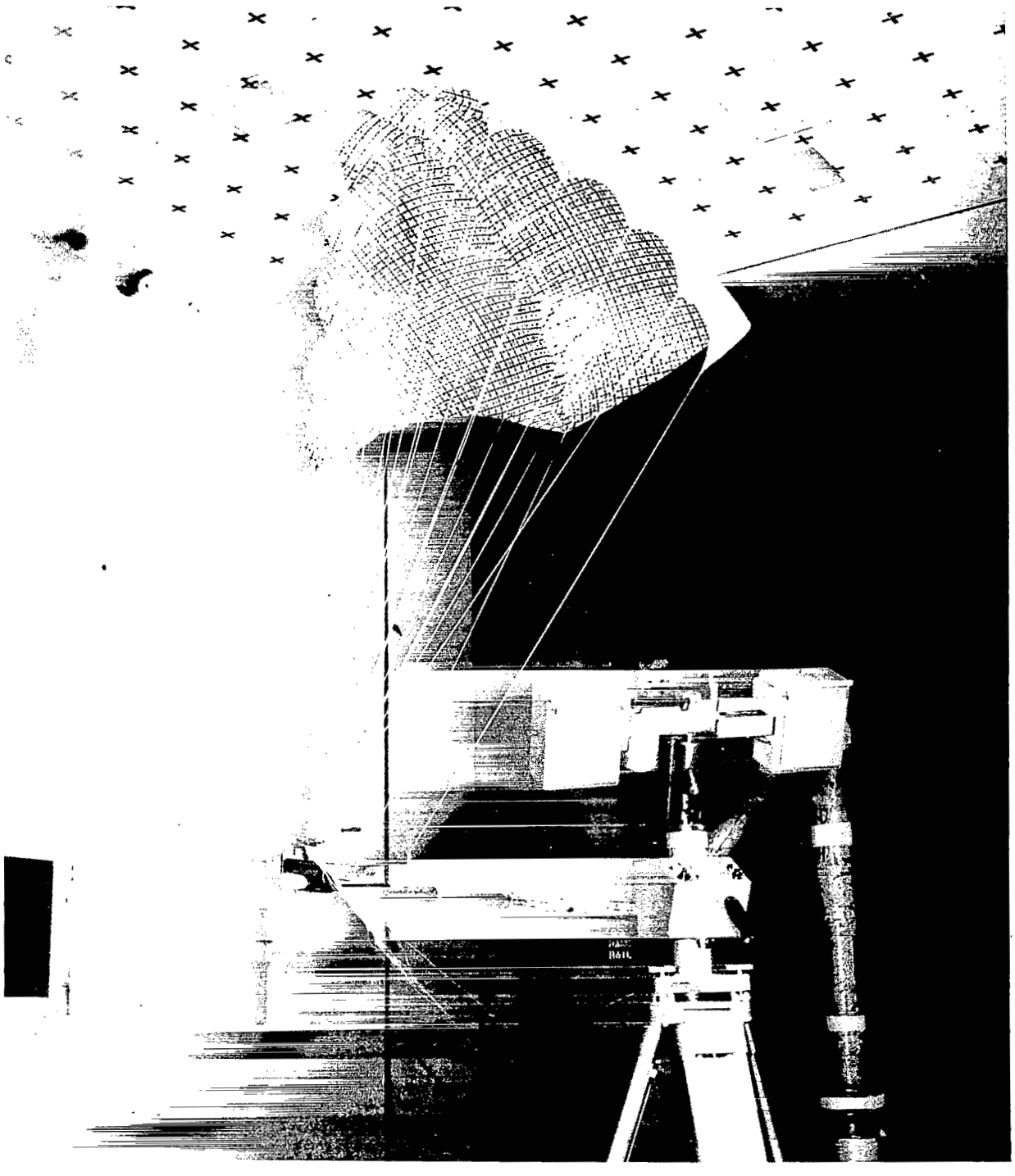

Figure 5.- Side view of setup for wind-tunnel tests. L-68-10 795

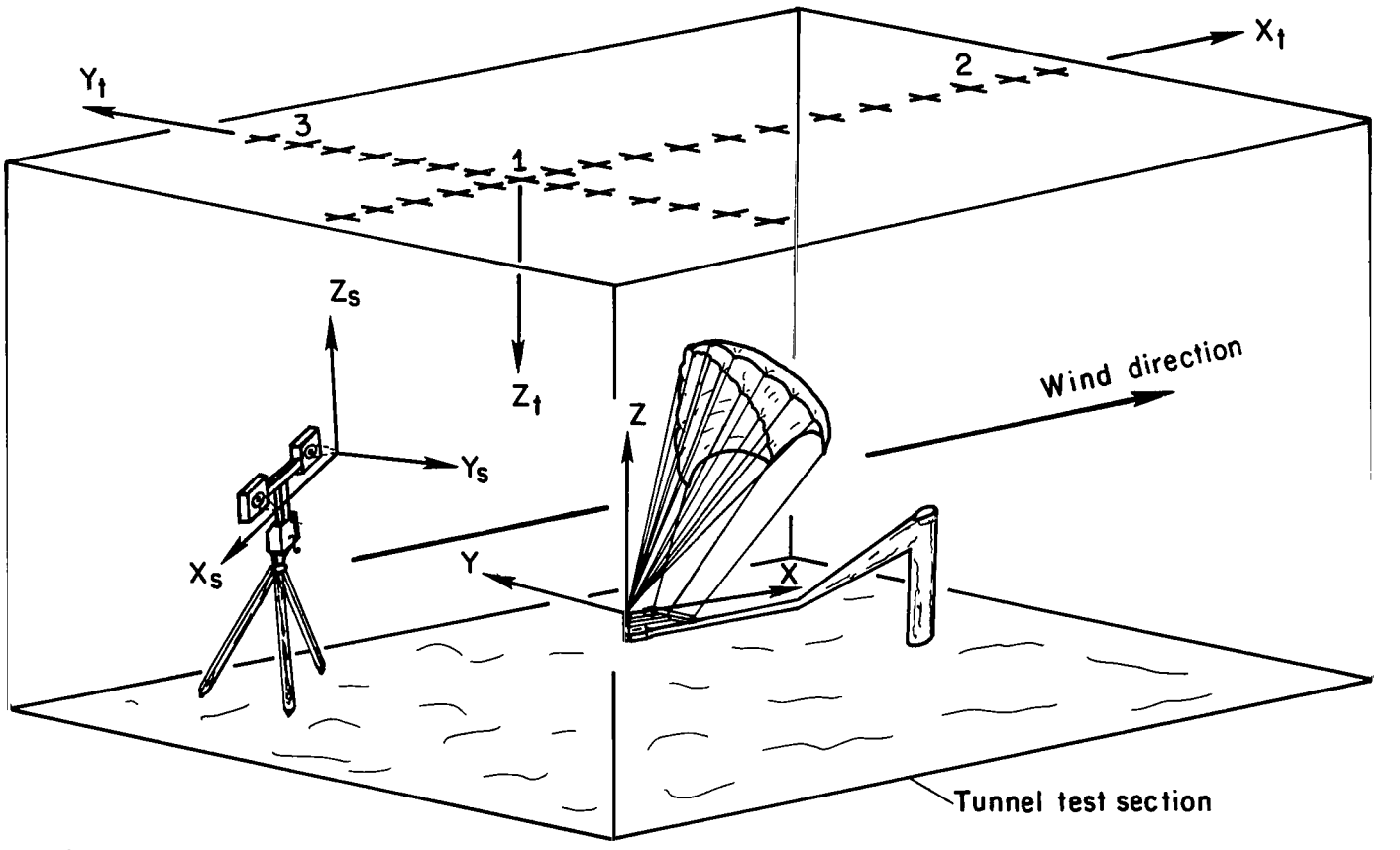

X_s, Y_s, Z_s — Camera axes

X_t, Y_t, Z_t — Tunnel axes

X, Y, Z, — Confluence-point axes

Figure 6.- Coordinate systems used in the transformation of shape data.

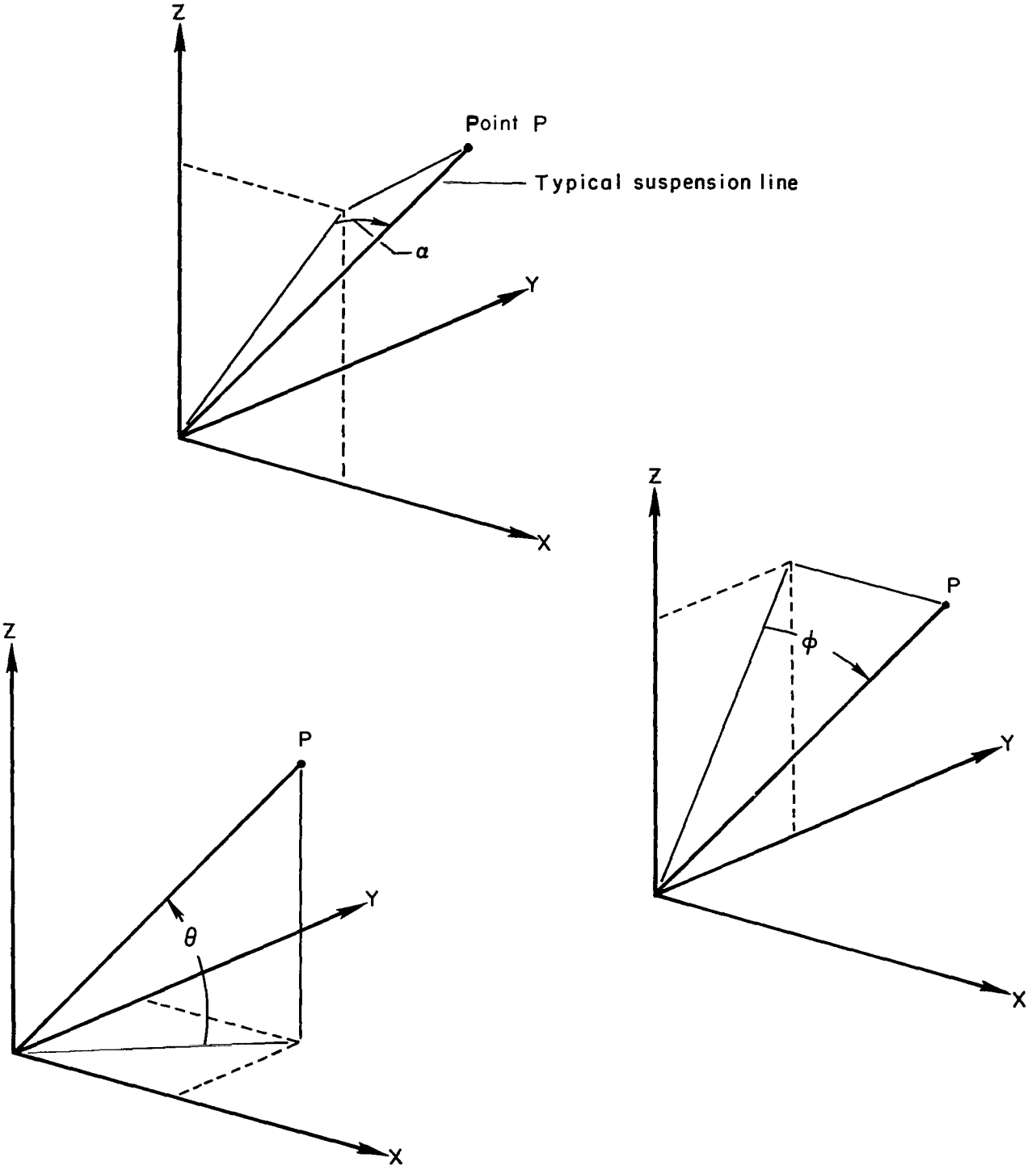

Figure 7.- Direction angles of a typical suspension line in the confluence-point axis system.

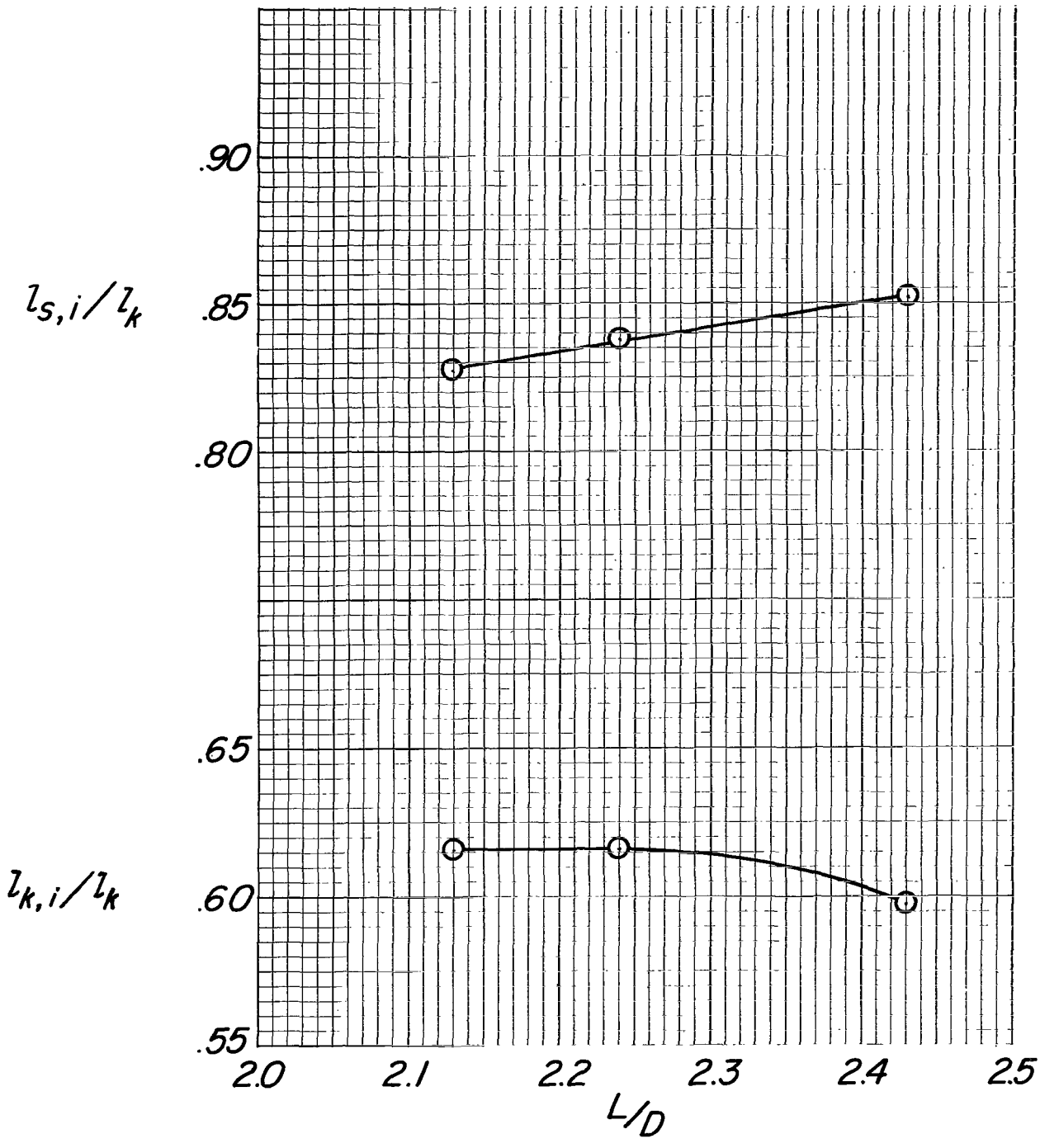

Figure 8.- Inflated span and inflated keel length as functions of lift-drag ratio.

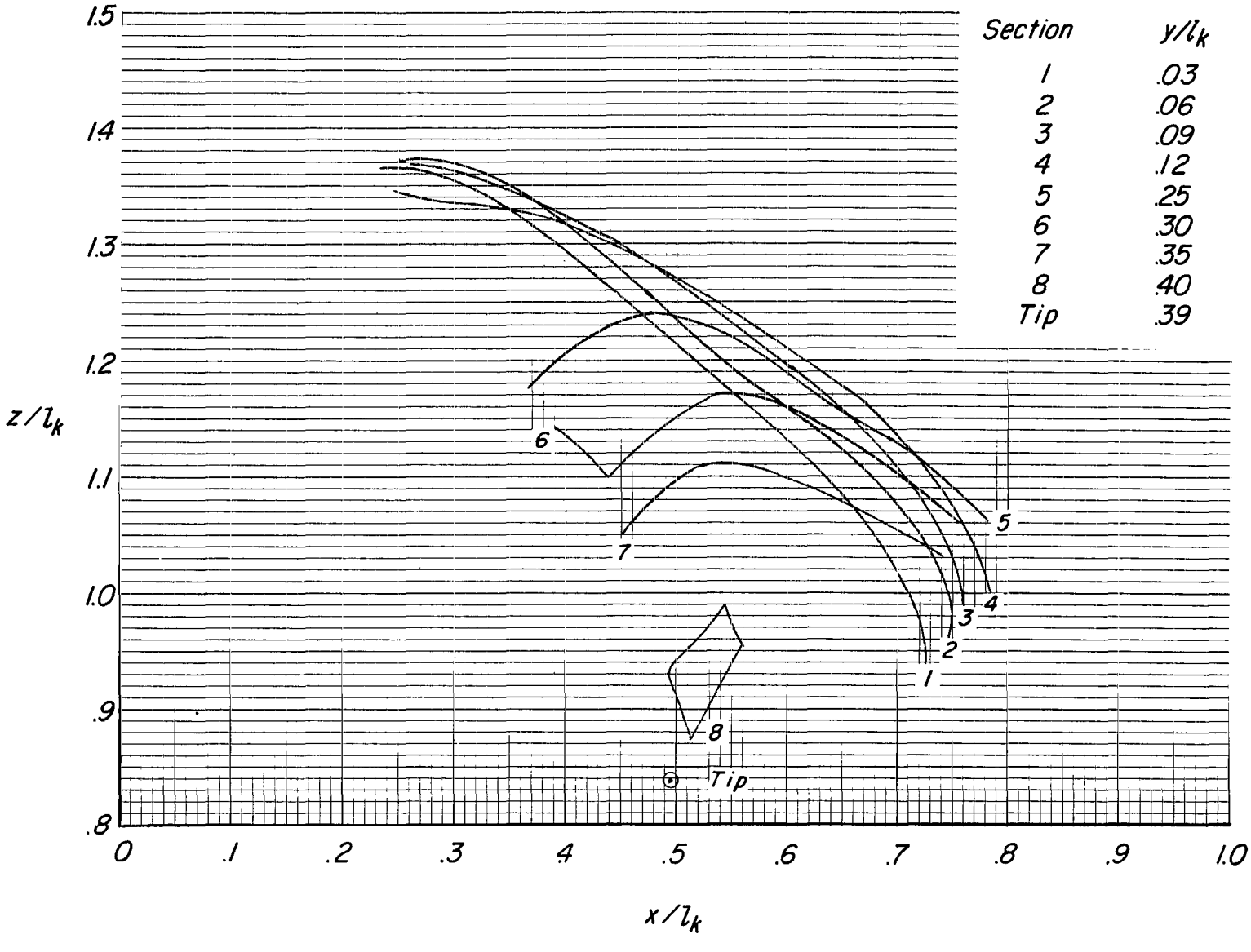

Figure 9.- Typical streamwise sections for a parawing flying at a lift-drag ratio of 2.24.

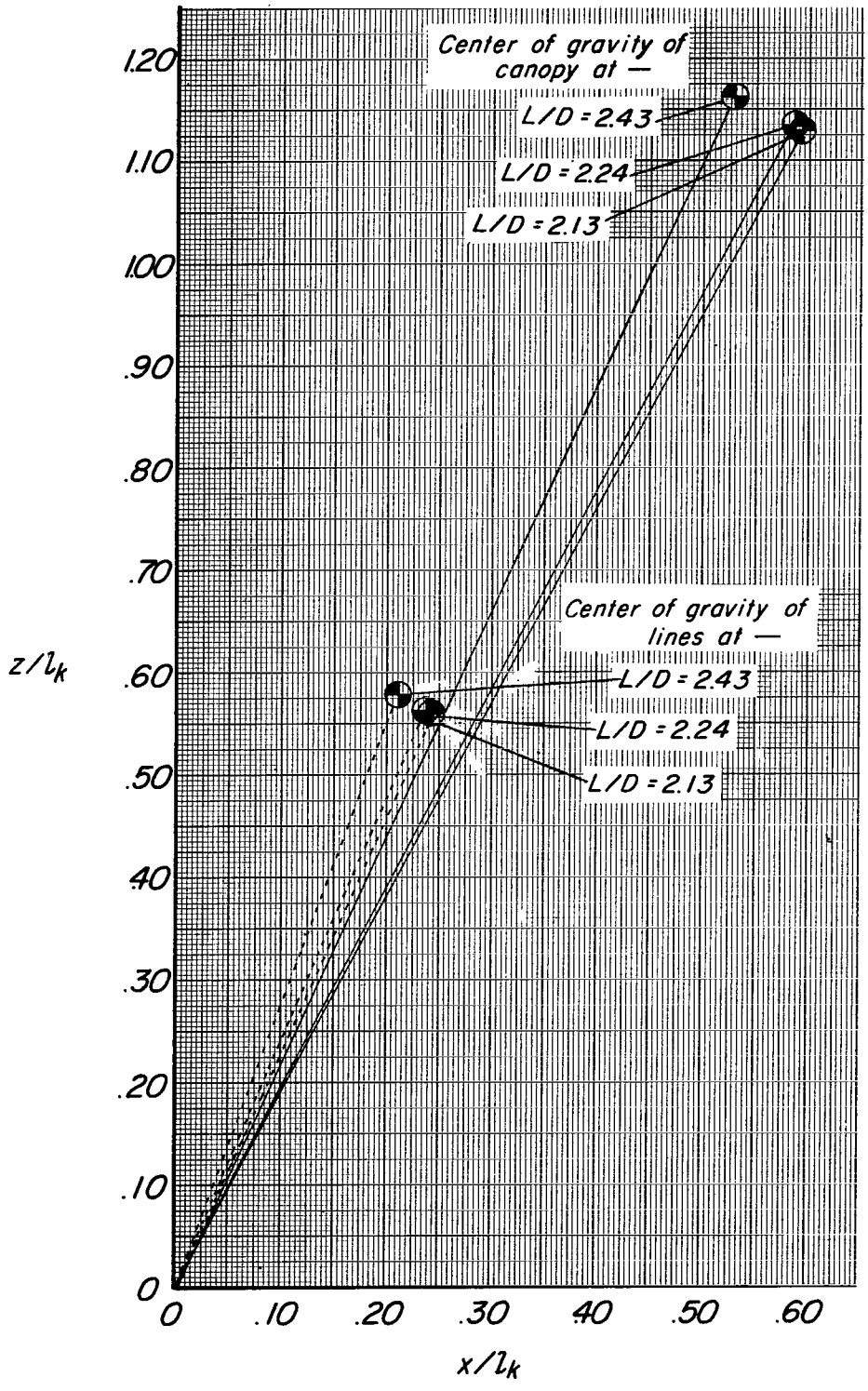

Figure 10.- Effect of changes in lift-drag ratio on center-of-gravity locations.

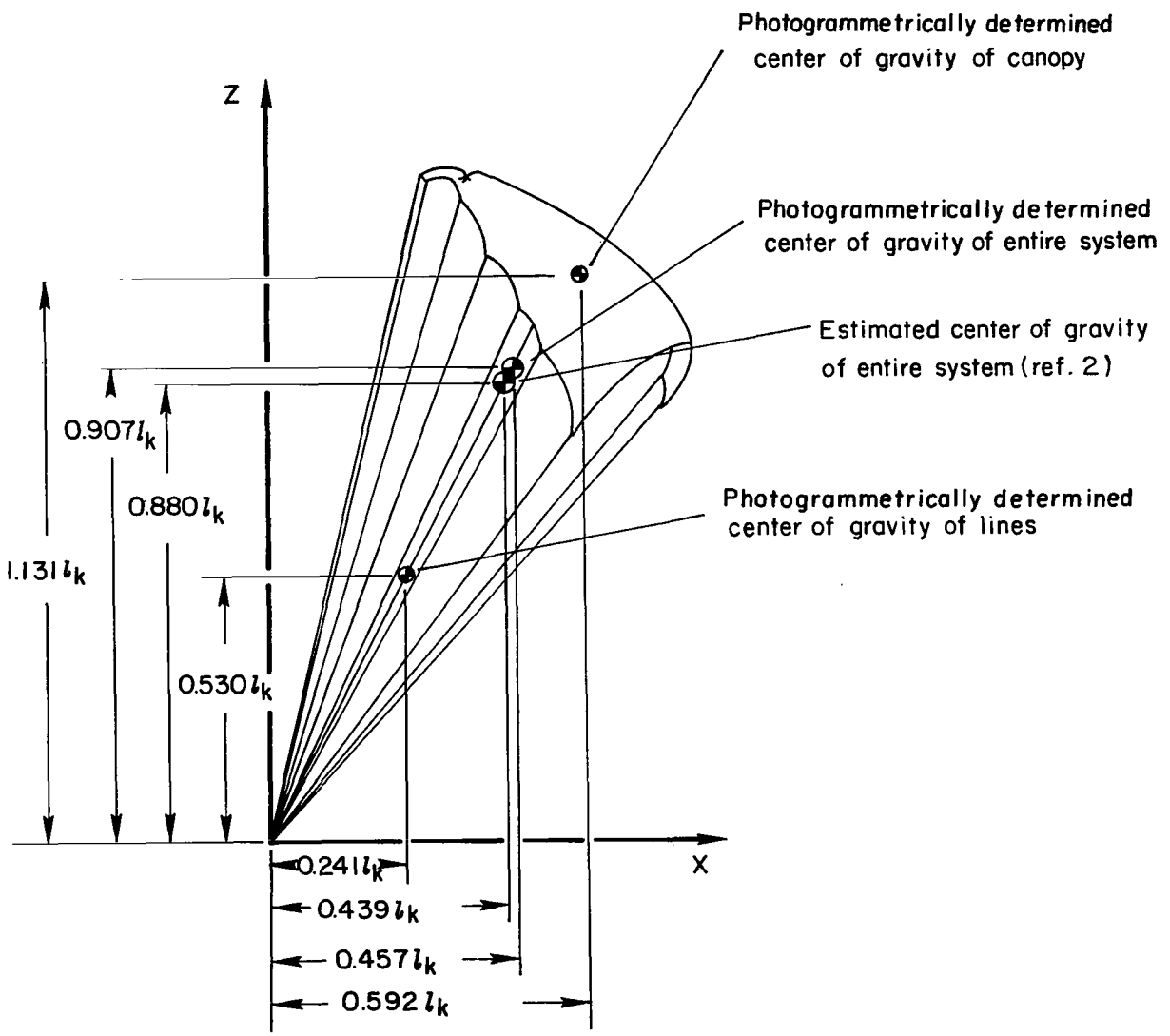

Figure 11.- Comparison of photogrammetrically determined and estimated center-of-gravity locations of a 24-foot (7.32-meter) parawing.

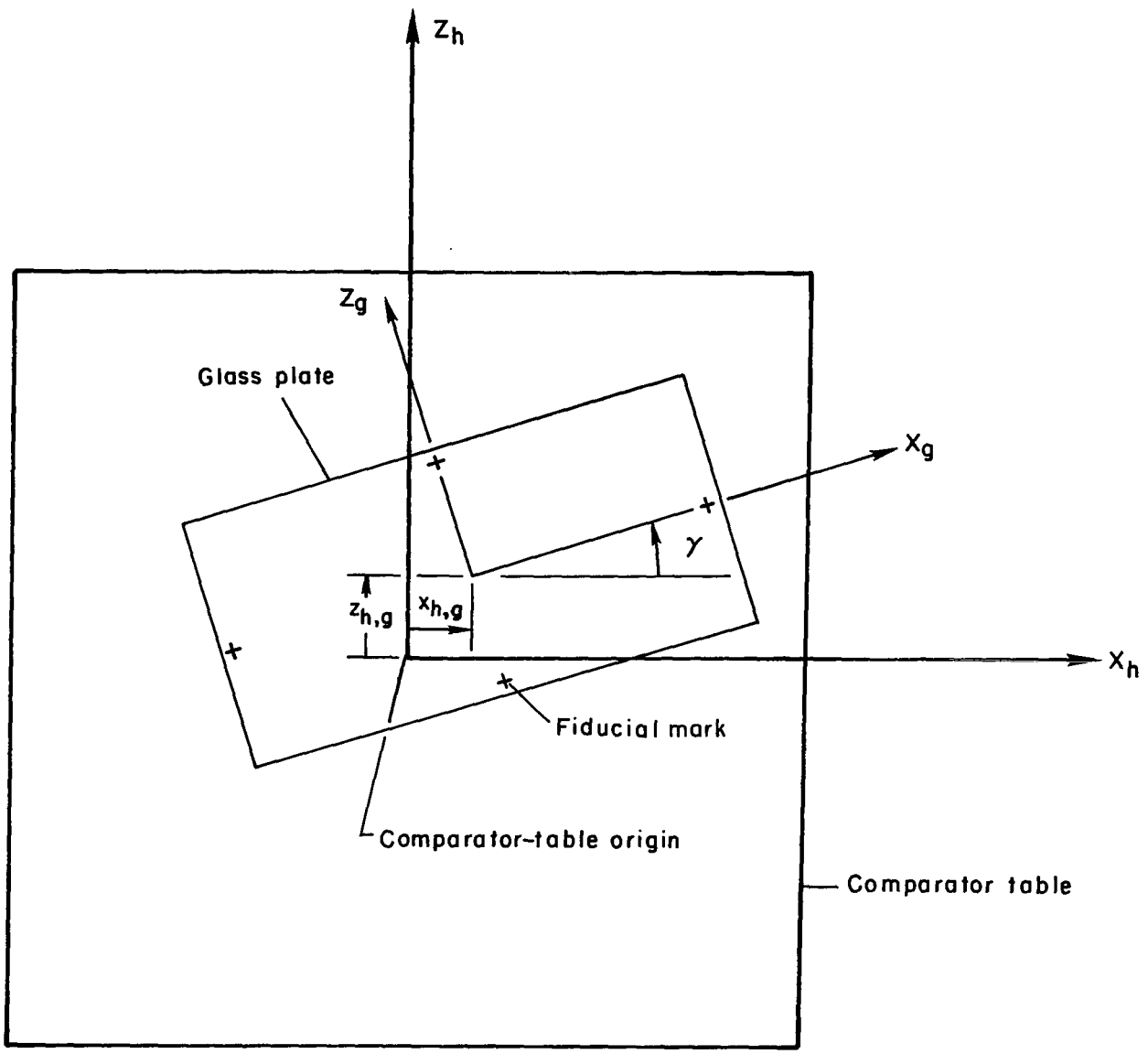

Figure 12.- Typical comparator-table setup.

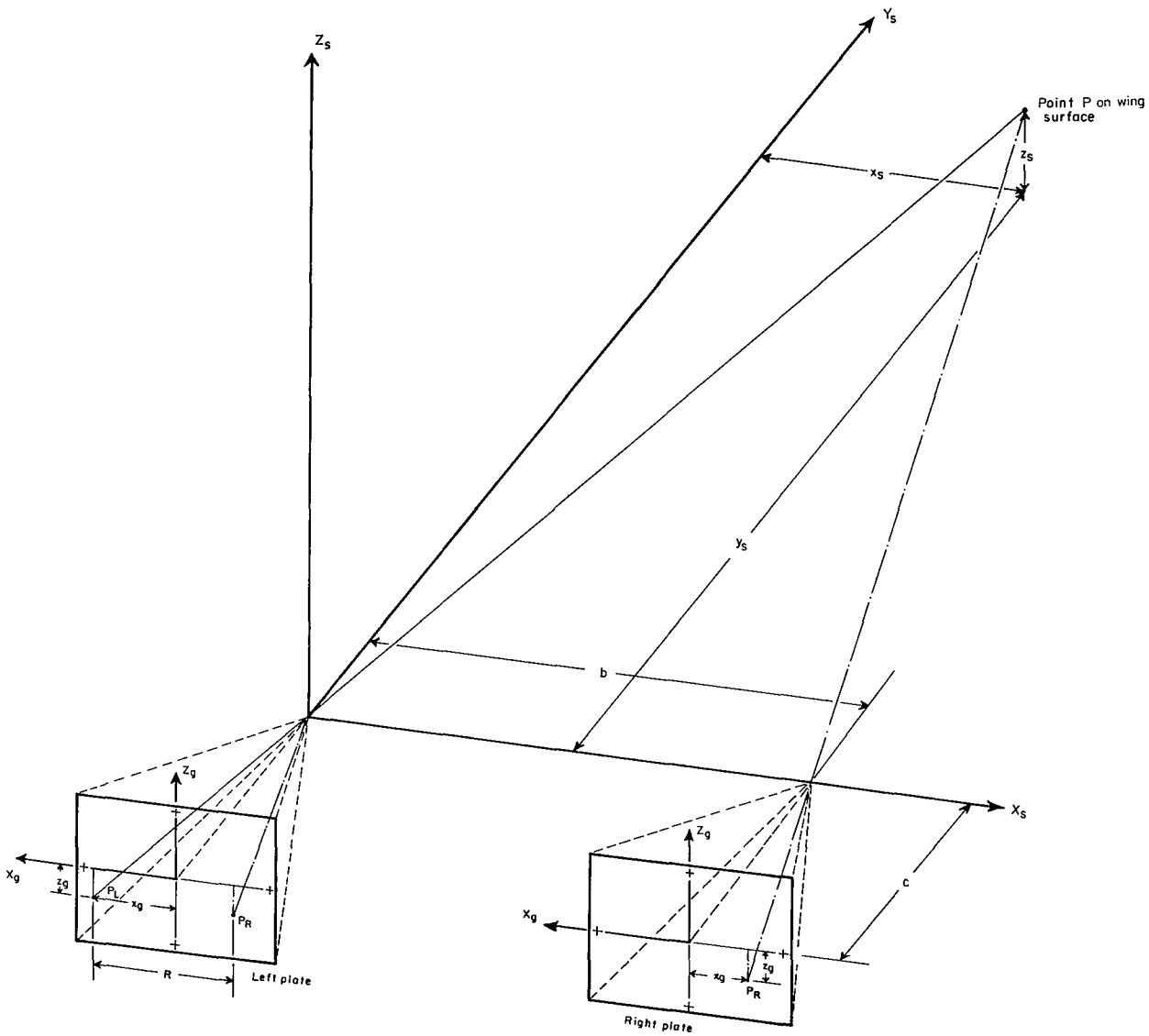

Figure 13.- Geometric relationships between two-dimensional glass-plate and three-dimensional camera coordinates.

NATIONAL AERONAUTICS AND SPACE ADMINISTRATION
WASHINGTON, D.C. 20546

OFFICIAL BUSINESS

FIRST CLASS MAIL

POSTAGE AND FEES PAID
NATIONAL AERONAUTICS AND
SPACE ADMINISTRATION

05U 001 26 51 3DS 70165 00903
AIR FORCE WEAPONS LABORATORY /WLOL/
KIRTLAND AFB, NEW MEXICO 87117

ATT E. LOU BOWMAN, CHIEF,TECH. LIBRARY

POSTMASTER: If Undeliverable (Section 158 Postal Manual) Do Not Return

"The aeronautical and space activities of the United States shall be conducted so as to contribute . . . to the expansion of human knowledge of phenomena in the atmosphere and space. The Administration shall provide for the widest practicable and appropriate dissemination of information concerning its activities and the results thereof."

—NATIONAL AERONAUTICS AND SPACE ACT OF 1958

NASA SCIENTIFIC AND TECHNICAL PUBLICATIONS

TECHNICAL REPORTS: Scientific and technical information considered important, complete, and a lasting contribution to existing knowledge.

TECHNICAL NOTES: Information less broad in scope but nevertheless of importance as a contribution to existing knowledge.

TECHNICAL MEMORANDUMS: Information receiving limited distribution because of preliminary data, security classification, or other reasons.

CONTRACTOR REPORTS: Scientific and technical information generated under a NASA contract or grant and considered an important contribution to existing knowledge.

TECHNICAL TRANSLATIONS: Information published in a foreign language considered to merit NASA distribution in English.

SPECIAL PUBLICATIONS: Information derived from or of value to NASA activities. Publications include conference proceedings, monographs, data compilations, handbooks, sourcebooks, and special bibliographies.

TECHNOLOGY UTILIZATION PUBLICATIONS: Information on technology used by NASA that may be of particular interest in commercial and other non-aerospace applications. Publications include Tech Briefs, Technology Utilization Reports and Notes, and Technology Surveys.

Details on the availability of these publications may be obtained from:

SCIENTIFIC AND TECHNICAL INFORMATION DIVISION

NATIONAL AERONAUTICS AND SPACE ADMINISTRATION

Washington, D.C. 20546